

The Possibility of the Kelvin-Helmholtz Instability during Sedimentation of Dust Grains in the Protoplanetary Disk

Yukihiko HASEGAWA, and Toru TSURIBE

*Department of Earth and Space Science, Graduate School of Science, Osaka University, Toyonaka,
Osaka 560-0043*

hasegawa@vega.ess.sci.osaka-u.ac.jp, tsuribe@vega.ess.sci.osaka-u.ac.jp

(Received 2012 September 18; accepted 2012 December 11)

Abstract

In this paper, we reexamine the possibility of shear-driven turbulence during sedimentation of dust grains in the protoplanetary disk. The shear-driven turbulence is expected to occur before the onset of the gravitational instability for MMSN model. While according to previous studies without taking account of growth of dust grains, with the larger abundance of dust grains, the gravitational instability is indicated to occur before shear-driven turbulence. In this paper, the case with dust growth is considered, and it is found that the Kelvin-Helmholtz instability tends to occur before the gravitational instability even in the case with large abundance of dust grains. This is different from previous results without the dust growth.

Key words: instabilities — methods: numerical — planetary systems: protoplanetary disk — solar system: formation

1. Introduction

For the formation of planetesimals, growth and motion of dust grains in the protoplanetary disks are essential. In a typical scenario, dust grains settle toward the midplane, and a thin dust layer is supposed to form (Nakagawa et al. 1981; Nakagawa et al. 1986). The gravitational instability (GI) of a disk (Safronov 1969; Goldreich & Ward 1973; Sekiya 1983) is expected to occur when density in the disk exceeds the critical density that is given by

$$\rho_c = \frac{0.606 M_\odot}{r^3}, \quad (1)$$

where r is the heliocentric distance (Sekiya 1983, 1998). In order to resolve the problem of radial drift of meter-sized dust (Adachi et al. 1976), GI in the thin dust layer is essential. However, as dust grains settle toward the midplane, vertical dust density gradient increases.

In such a case, the vertical shear of the rotational velocity in the dust layer becomes strong. The strong shear is expected to induce the Kelvin-Helmholtz instability (KHI) (Chandrasekhar 1961). As a result, KHI is expected to induce shear-driven turbulence. It is considered that turbulence due to KHI prevents dust grains from settling further toward the midplane (Sekiya 1998; Sekiya & Ishitsu 2001; Michikoshi & Inutsuka 2006). Sekiya (1998) shows that GI does not occur in MMSN (minimum mass solar nebula) model (Hayashi 1981; Hayashi et al. 1985). On the other hand, Sekiya (1998) and Sekiya & Ishitsu (2001) show that turbulence induced by KHI becomes weaker if dust abundance in the protoplanetary disk is much larger than MMSN model. If turbulence is weak, GI will occur and planetesimals may form. To discuss the possibility of the shear-driven turbulence, Richardson number is known as an indicator of KHI (Chandrasekhar 1961). If the Richardson number is smaller than a critical value, KHI is expected to occur. Chandrasekhar (1961) showed that the critical value is 0.25, but Gómez & Ostriker (2005) and Johansen et al. (2006) showed that the inclusion of the Coriolis force yields a much higher critical Richardson numbers. Other than KHI, the dynamics of the midplane has been shown to be dominated by the streaming instability (Youdin & Goodman 2005; Johansen & Youdin 2007).

Investigations of the turbulence are essential for understanding the processes of the planetesimal formation, and there are many previous studies (Weidenschilling 1980; Cuzzi et al. 1993; Dobrovolskis 1999; Johansen & Youdin 2007; Bai & Stone 2010). These previous studies confirm the result that shows that GI is expected to occur before KHI if dust abundance is large. However, above previous studies did not take account of dust growth. Not only gas turbulence but also dust growth are essential to understand the planetesimal formation. Dust grains grow due to dust-dust collisions while they settle toward the midplane (Nakagawa et al. 1981; Nakagawa et al. 1986). Nakagawa et al. (1986) shows that the law of gas drag force on dust grains is changed in the process of sedimentation of dust grains because of dust growth. They also show that the change of the law of gas drag influences sedimentation of dust grains. Dust growth is strongly related to gas drag. However, it is difficult to simulate both dust growth and gas turbulence numerically because of the computer performance.

In this paper, we numerically calculate the sedimentation and the growth of dust grains, and the possibility of KHI is discussed using the distribution of dust density that is consistent with their sedimentation in the disk. In §2, the models of gas and dust grains of the protoplanetary disk in this paper are summarized. In §3, we show numerical results for sedimentation of dust grains without growth. In §4, results are shown for the case with dust growth. In §5, we discuss the effects neglected in this paper. In §6, we summarize our results.

2. Models of the protoplanetary disk

2.1. Disk model

For simplicity, we restrict ourselves to the case with $r = 1$ AU. The protoplanetary disk is composed of gas and dust. In this paper, the gas surface density Σ_g and the dust surface density Σ_d are assumed to be

$$\Sigma_g = 1.7 \times 10^3 f_g \left(\frac{r}{1[\text{AU}]} \right)^{-\frac{3}{2}} [\text{g cm}^{-2}], \quad (2)$$

$$\Sigma_d = 7.1 f_d \xi_{\text{ice}} \left(\frac{r}{1[\text{AU}]} \right)^{-\frac{3}{2}} [\text{g cm}^{-2}], \quad (3)$$

where f_g , f_d and ξ_{ice} are parameters of abundance for gas, dust and condensed water ice, respectively (Hayashi 1981; Hayashi et al. 1985). At $r = 1$ AU, $\xi_{\text{ice}} = 1$. The case with $f_g = 1$ and $f_d = 1$ corresponds to MMSN model. In this paper, we consider the case with $f_g = 1$ and various f_d . In MMSN model, temperature T is given by

$$T = 280 \left(\frac{r}{1[\text{AU}]} \right)^{-\frac{1}{2}} [\text{K}]. \quad (4)$$

2.2. Gas properties

In this paper, we assume that the gas component is in hydrostatic equilibrium in the vertical direction without self-gravity. In this case, the gas density is given by

$$\rho_g(z) = \frac{\Sigma_g}{\sqrt{\pi} H_g} \exp \left[- \left(\frac{z}{H_g} \right)^2 \right], \quad (5)$$

where z is the height from the midplane of the disk and H_g is the scale height of the disk given by

$$H_g \equiv \frac{\sqrt{2} c_s}{\Omega_K} = 4.7 \times 10^{-2} \left(\frac{r}{1[\text{AU}]} \right)^{\frac{5}{4}} [\text{AU}]. \quad (6)$$

The symbol Ω_K is Keplerian angular velocity. The symbol c_s is the sound velocity as

$$c_s = \sqrt{\frac{k_B T}{m_\mu}} = 0.99 \left(\frac{r}{1[\text{AU}]} \right)^{-\frac{1}{4}} [\text{km s}^{-1}], \quad (7)$$

where k_B is the Boltzmann constant and $m_\mu (= 3.9 \times 10^{-24} \text{ g})$ is the mass of gas molecular (the mean molecular weight is 2.34). The mean free path of gas molecules, l_g , is given by $l_g = 1.44 \text{ cm}$ at $r = 1$ AU (Nakagawa et al. 1986). From equation (6), the protoplanetary disk is geometrically thin.

2.3. Dust properties

In this paper, dust grains are assumed to be compact and spherical with radius s . In the case with $s \leq 3l_g/2 = 2.2 \text{ cm}$, the gas drag force is given by Epstein's law. In this case, at

$r = 1$ AU and $z = 0$, the stopping time t_{stop} is given by

$$t_{\text{stop}} = \frac{\rho_s}{\rho_g(z)} \frac{s}{c_s} = 1.5 \times 10^{-3} \left(\frac{f_g}{1} \right)^{-1} \left(\frac{\rho_s}{3[\text{g cm}^{-3}]} \right) \left(\frac{s}{2.2[\text{cm}]} \right) [\text{year}], \quad (8)$$

where ρ_s is the internal density of the dust grain. In the case with $s \geq 3l_g/2$, gas drag is given by Stokes' law and the stopping time is given as

$$t_{\text{stop}} = \frac{2}{3} \frac{\rho_s}{\rho_g(z)} \frac{s^2}{l_g c_s} = 1.5 \times 10^{-3} \left(\frac{l_g f_g}{1.4[\text{cm}]} \right)^{-1} \left(\frac{\rho_s}{3[\text{g cm}^{-3}]} \right) \left(\frac{s}{2.2[\text{cm}]} \right)^2 [\text{year}], \quad (9)$$

at $r = 1$ AU and $z = 0$. In this paper, we adopt the criterion $s \leq 3l_g/2$ for the validity of the Epstein regime while there are also previous studies that use $s \leq 9l_g/4$ (e.g., Youdin & Shu 2002).

In this paper, we assumed that radial motion of dust grains can be neglected (Nakagawa et al. 1981). The equation of motion of a dust grain in the vertical direction is given by

$$\frac{dv_z}{dt} = -\frac{v_z}{t_{\text{stop}}} - \Omega_K^2 z, \quad (10)$$

where t is the time and v_z is the vertical velocity of the dust grain. We assume that gas are not affected by dust grains and gas density is always given by equation (5). In this paper, we approximate vertical velocity of dust grains by the terminal velocity (Nakagawa et al. 1981; Nakagawa et al. 1986). With setting $dv_z/dt = 0$ in equation (10), we obtain a terminal velocity of a dust grain as

$$v_z(z) = -t_{\text{stop}} \Omega_K^2 z. \quad (11)$$

2.4. The mixture of gas and dust grains

In this paper, we use a single-fluid approximation for the azimuthal motion. The rotational velocity of a mixed fluid of gas and dust is given as

$$v_\phi = \left[1 - \frac{\rho_g(z)}{\rho_g(z) + \rho_d(z)} \eta \right] v_K. \quad (12)$$

In equation (12), ρ_d is the dust density, v_K is the circular Keplerian velocity, and

$$\eta = -\frac{1}{4} \frac{H_g^2}{r^2} \frac{\partial \ln P}{\partial \ln r}, \quad (13)$$

where $P = c_s^2 \rho_g$ is the gas pressure. Using equations (2), (5), (6) and (7), we have

$$\eta = \frac{13}{16} \left(\frac{H_g}{r} \right)^2 = 1.8 \times 10^{-3} \left(\frac{r}{1[\text{AU}]} \right)^{\frac{1}{2}} \ll 1. \quad (14)$$

2.5. Richardson number

To discuss the possibility of the shear-driven turbulence, we calculate Richardson number that is the indicator of KHI (Chandrasekhar 1961). The Richardson number is given by

$$\text{Ri} = -\frac{g_z}{\rho_g(z) + \rho_d(z)} \left[\frac{\partial \rho_g(z)}{\partial z} + \frac{\partial \rho_d(z)}{\partial z} \right] \left(\frac{\partial v_\phi}{\partial z} \right)^{-2}, \quad (15)$$

where g_z is the gravitational acceleration given by $g_z = \Omega_K^2 z$ (Sekiya & Ishitsu 2001). Equation (15) is based on an assumption that the disk is composed of an incompressible one component fluid for simplicity. We use equation (15) as an indicator of KHI for simplicity. If Ri is smaller than the critical value Ri_c , KHI is expected to be induced in the protoplanetary disk, and it is expected that the laminar flow of the mixed fluid in the disk becomes turbulent. Chandrasekhar (1961) showed that $\text{Ri}_c = 0.25$, but Gómez & Ostriker (2005) and Johansen et al. (2006) showed that the inclusion of the Coriolis force yields a much higher critical Richardson numbers. In this paper, we use a value $\text{Ri}_c = 0.25$, but in the subsequent section we will discuss the case with $\text{Ri}_c = 0.8$ (Johansen et al. 2006).

By seeing equations (12) and (15), Ri depends on the distribution of dust density. In this paper, we calculate Richardson number for the dust density given by numerical calculations in each time.

2.6. The growth and sedimentation of dust grains

The growth and sedimentation of dust grains is described by

$$\begin{aligned} \frac{\partial}{\partial t} n(m, z) + \frac{\partial}{\partial z} [n(m, z) v_z(m, z)] \\ = -n(m, z) \int_0^\infty A(m, m', z) n(m', z) dm' \\ + \frac{1}{2} \int_0^m [A(m - m', m', z) n(m - m', z) n(m', z) dm'], \end{aligned} \quad (16)$$

where $n(m, z)dm$ is the number density of the dust grains with mass between m to $m + dm$ at the height z and $A(m, m', z)$ is the coalescence rate for two dust grains with m and m' at z . The symbol $n(m, z)dz$ gives a mass function in z to $z + dz$. The dust density at z , $\rho_d(z)$, is given by

$$\rho_d(z) = \int_0^\infty m n(m, z) dm. \quad (17)$$

As for velocity which induces dust-dust collisions, velocities generated during sedimentation and the thermal Brownian motion are considered. The relative velocities of two dust grains due to sedimentation Δv_s and to the thermal motion Δv_B is given by

$$\Delta v_s = |v_z(m, z) - v_z(m', z)|, \quad (18)$$

$$\Delta v_B = \sqrt{k_B T} \sqrt{\frac{1}{m} + \frac{1}{m'}}, \quad (19)$$

respectively. We assume that the coalescence rate $A(m, m', z)$ is given by

$$A(m, m', z) = \pi(s + s')^2 (\Delta v_s + \Delta v_B) p_s, \quad (20)$$

where p_s is the coalescence probability and p_s is assumed to be 1 as in Nakagawa et al. (1981).

For simplicity, we ignore the bouncing barrier (Zsom et al. 2010) and the electrostatic barrier (Okuzumi 2009).

Integrating equation (16) with respect to m , we have

$$\frac{\partial}{\partial t} \int_0^\infty mn(m, z) dm + \frac{\partial}{\partial z} \int_0^\infty mn(m, z) v_z(m, z) dm = 0. \quad (21)$$

Using equations (17) and (21), we have

$$\frac{\partial}{\partial t} \rho_d(z) + \frac{\partial}{\partial z} [\rho_d(z) \bar{v}_z(z)] = 0, \quad (22)$$

which is the continuity equation for dust grains treated as fluid, where the mean sedimentation velocity of dust fluid at z is given by

$$\bar{v}_z(z) = \frac{\int_0^\infty v_z(z) mn(m, z) dm}{\int_0^\infty mn(m, z) dm}. \quad (23)$$

3. Sedimentation of dust grains without growth

In this section, in order to clarify the effect of dust growth, we first consider the case at $r = 1$ AU without the growth.

3.1. The initial condition

In this paper, dust density $\rho_d(z)$ is assumed to be symmetric to the midplane, so we examine only the region of $z \geq 0$. As initial condition, the initial density of dust is assumed to be

$$\rho_d(z) = \frac{\Sigma_d}{\sqrt{\pi} H_d} \exp \left[- \left(\frac{z}{H_d} \right)^2 \right], \quad (24)$$

where H_d is time dependent scale height of dust density profile with $H_d = H_g$ at $t = 0$.

In this paper, we assume the same initial functional form for $\rho_g(z)$ and $\rho_d(z)$, and we neglect the dependence of v_K on z . Note that $\text{Ri} = \infty$ at $t = 0$ from equation (15), i.e., initial state is stable against KHI. This is because the rotational velocity of the mixed fluid of gas and dust grains v_ϕ at $t = 0$ is independent of z (cf. equation (12)), i.e., $\partial v_\phi / \partial z = 0$ in equation (15).

3.2. Sedimentation of dust grains with single size

First, we consider the sedimentation of dust grains with a single size. We assume that all dust grains are small enough and that the drag force is given by Epstein's law. The characteristic time scale for sedimentation of dust grains is given by

$$t_{\text{sed}} \equiv \frac{z}{|v_z(z)|} = \frac{1}{t_{\text{stop}} \Omega_K^2}. \quad (25)$$

From equations (8) and (25), it is shown that the characteristic time scale of sedimentation is much larger than the Keplerian period $t_{\text{sed}} \Omega_K \gg 1$ in the case when the stopping time is much smaller than the Keplerian period $t_{\text{stop}} \Omega_K \ll 1$. In such a case with a single size without dust growth, profile of dust density evolves in a self-similar manner (Garaud & Lin 2004). Here,

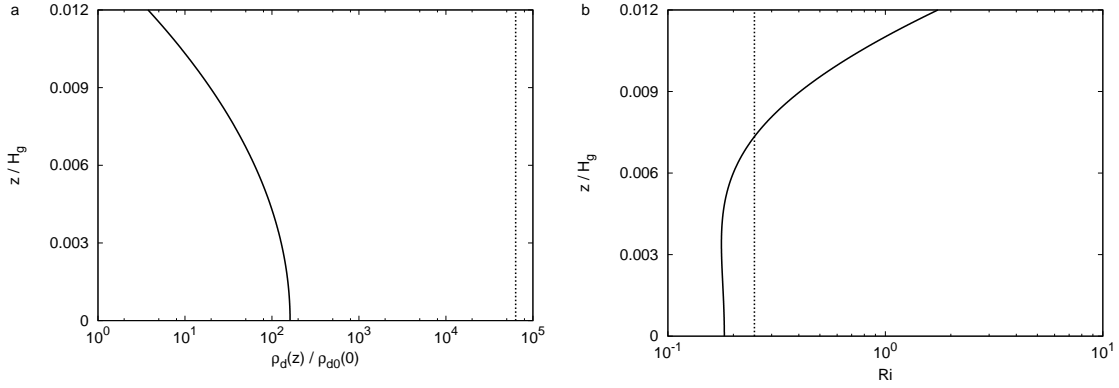


Fig. 1. Dust density and Richardson number at $r = 1$ AU for the case when dust grains have a single size with $f_d = 1$. (a) The distribution of dust density (solid line). The abscissa shows the dust density $\rho_d(z)$ in unit of $\rho_{d0}(0)$. The ordinate shows z coordinates in unit of H_g . The critical density ρ_c is also drawn (dotted line). (b) The distribution of Richardson number (solid line). The abscissa shows Richardson number. The ordinate shows z coordinates in unit of H_g . The critical value Ri_c is also drawn (dotted line).

during sedimentation of dust, the distribution of gas density assumed to be constant remain as equation (5). When the time evolution of dust density proceeds in a self-similar manner, dust density profile in $t > 0$ is also given by equation (24) with temporally decreasing $H_d(t)$ with $0 < H_d(t) \leq H_g$. Using equations (5), (12) and (24), we have

$$\frac{\partial v_\phi}{\partial z} = 2\eta z v_K \left(\frac{1}{H_g^2} - \frac{1}{H_d^2} \right) \frac{\rho_g(z)\rho_d(z)}{[\rho_g(z) + \rho_d(z)]^2}. \quad (26)$$

Substituting (14) and (26) into (15), an analytical formula for Richardson number can be derived.

Figure 1 shows results of distribution of dust density and Richardson number when $\rho_d(0) \simeq 160\rho_{d0}(0)$ for the case with $f_d = 1$, where H_d is $0.0062H_g$. We define the initial value of dust density at the midplane as $\rho_{d0}(0) \equiv \Sigma_d/(\sqrt{\pi}H_g)$. In Figure 1, it is seen that dust density at the midplane is much smaller than the critical density $\rho_c = 6.3 \times 10^4 \rho_{d0}(0)$, and that Richardson number is smaller than $Ri_c = 0.25$ around the midplane ($z/H_g \lesssim 0.0075$). Thus, KHI is expected before GI in this case with $f_g = f_d = 1$ at $r = 1$ AU.

Assuming equilibrium condition for KHI, previous studies have shown that GI tends to occur if dust abundance in the protoplanetary disk is much larger than MMSN model (Sekiya 1998; Sekiya & Ishitsu 2001). Now using non-equilibrium time dependent density profile during sedimentation, we consider the possibility for GI in the case with large f_d . We seek the condition of dust abundance f_d by which GI occurs before the onset of KHI. In Figure 1 (a), it is seen that the distribution of dust density has a maximum value at the midplane. When f_d is larger than 1, the dotted line in Figure 1 (a) moves to left because the abscissa is inversely proportional to $\rho_{d0}(0) \propto f_d$. Dust density at the midplane is the first to reach the critical density for GI

because time development of dust density proceeds in a self-similar manner. A characteristic H_d when dust density at midplane attains ρ_c can be obtained from equation (24). We define the characteristic H_d as H_c . With substituting 0, H_d and ρ_c for z , H_g and $\rho_d(z)$ in equation (24), respectively, H_c is given by

$$H_c = \frac{\Sigma_d}{\sqrt{\pi}\rho_c} = 1.6 \times 10^{-5} f_d H_g \propto f_d. \quad (27)$$

From Figure 1 (b), it is found that the distribution of Richardson number has a local minimum value at $z/H_g = 3.5 \times 10^{-3}$. The height where distribution of Richardson number takes the local minimum value is defined as z_c . At $z = z_c$, from $\partial \text{Ri} / \partial z|_{z=z_c} = 0$, we find

$$\rho_g(z_c) = 2\rho_d(z_c), \quad (28)$$

with assuming $H_d/H_g \ll 1$. From equation (28), z_c is given as

$$z_c = \left[\ln \left(\frac{2\Sigma_d}{\Sigma_g} \frac{H_g}{H_d} \right) \right]^{\frac{1}{2}} H_g. \quad (29)$$

Richardson number at $z = z_c$ is given by

$$\text{Ri}(z = z_c) = \frac{27}{8} \left(\frac{H_d}{\eta r} \right)^2, \quad (30)$$

with assuming $H_d/H_g \ll 1$. From equations (27), (28) and (30), the condition of dust abundance f_d that is necessary for GI to occur before KHI is derived as

$$f_d = \left[\frac{8\pi}{27} \text{Ri}(z = z_c) \right]^{\frac{1}{2}} \eta r \rho_c \left(\frac{\Sigma_d}{f_d} \right)^{-1} \geq 6.6 \times 10^2, \quad (31)$$

at $r = 1$ AU and $f_g = 1$. Note that $\Sigma_d \propto f_d$.

In Figure 2, results for the case with $f_d = 6.6 \times 10^2$ are shown. In Figure 2, it is seen that dust density at the midplane indeed attains the critical density ρ_c and that Richardson number remains marginally larger than the critical value Ri_c . Thus, in the case when dust grains have a single size and don't grow at $r = 1$ AU with $f_g = 1$, GI is expected to occur before KHI only if the dust surface density is much larger than the gas surface density.

This tendency is similar to the result of Sekiya (1998), but the value of f_d in this paper ($f_d = 6.6 \times 10^2$) is larger than the value in Sekiya (1998) ($f_d = 16.8$). The value of f_d in Sekiya (1998) corresponds to the condition that the protoplanetary disk is in a quasi-equilibrium state for KHI. On the other hand, the value in this paper corresponds to the condition that GI occurs before KHI during sedimentation and that is more stringent. Therefore, the value of f_d in this paper is larger than the value in Sekiya (1998).

3.3. The effect of size distribution

Next, we consider the sedimentation of dust grains with initial size distribution but without growth. The result given by equation (31) is independent of dust radius as long as the stopping time is given by Epstein's law. Now we consider the effect of initial size distribution of

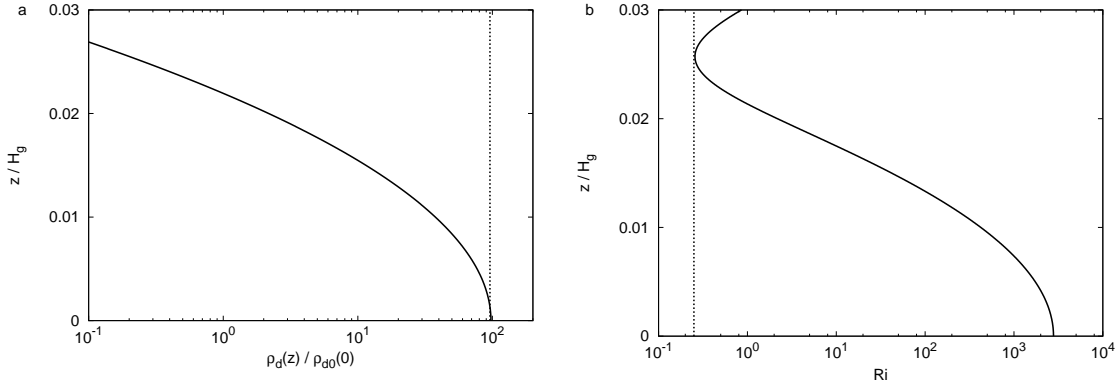


Fig. 2. Same as Figure 1, but for the case with $f_d = 6.6 \times 10^2$.

dust grains. Characteristic time scale for sedimentation of dust grains in equation (25) depends on size of dust grains. Thus, even in the same time, scale height of dust density profile for different size of dust grains is different. Therefore, it is expected that total dust density profile will change from initial Gaussian profile in the case when dust grains have a size distribution. We consider N_d kinds of dust grains with different radius. For simplicity, we consider the case when s is given by integer multiples of the minimum radius of dust grains s_0 and when the maximum value s_{\max} is given by $N_d s_0$.

In order to derive the scale height $H_{d,s}$ of dust density profile for dust grains with a radius s , we assume that $\rho_g(z)$ is uniform for simplicity. The stopping time of dust grains $t_{\text{stop}} = (\rho_s/\rho_g)(s/c_s)$ is proportional to s and is constant with z . The vertical velocity of dust grains $v_z(z) \propto t_{\text{stop}} z$ is proportional to s and to z . From the time evolution of $z(t)$ with different radius of dust grains with $z = H_g$ at $t = 0$, the formula for $H_{d,s}$ can be derived as

$$\frac{H_{d,s}}{H_g} = \left(\frac{H_{d,s_0}}{H_g} \right)^{s/s_0}. \quad (32)$$

In equation (32), it is seen that $H_{d,s}$ is determined only by H_{d,s_0} and s/s_0 instead of s because radii of all dust grains are normalized by the smallest dust grains.

The distribution of total dust density $\rho_d(z)$ is given as

$$\rho_d(z) = \sum_{s/s_0=1}^{N_d} \rho_d(s, z), \quad (33)$$

where $\rho_d(s, z)$ is the density of dust grains with radius s at z . For simplicity, initial size distribution is assumed to be a power law of dust radius,

$$n_d(s, z) = n_d(s_0, z) \left(\frac{s}{s_0} \right)^p, \quad (34)$$

where $n_d(s, z)$ is the initial condition of the number density for radius s at z with a power index p . We assume $p = -3$ for simplicity. In the case with $p = -3$, $s^3 n_d(s, z)$ is equal to $s_0^3 n_d(s_0, z)$ from equation (34). Then, initial condition of $\rho_d(s, z)$ is given by

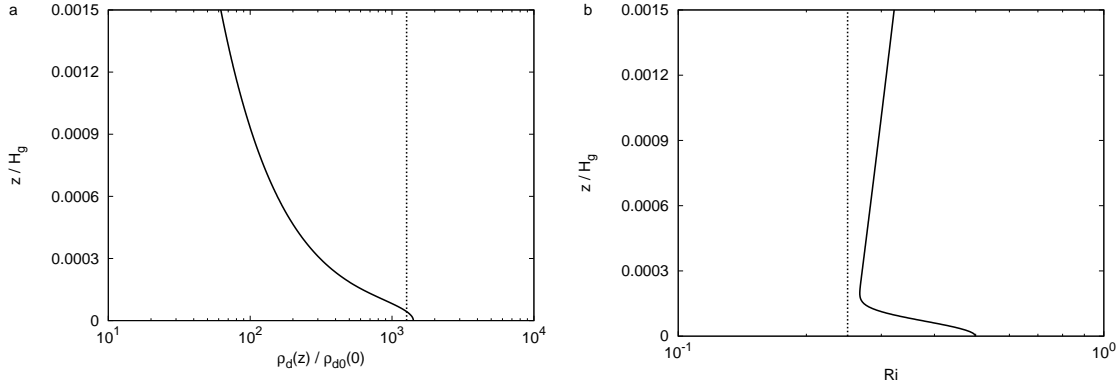


Fig. 3. Dust density and Richardson number at $r = 1$ AU for the case when dust grains have a size distribution with $f_d = 50$. Lines, abscissas and ordinates show the same as ones of Figure 1.

$$\rho_d(s, z) = \frac{4}{3}\pi\rho_s s^3 n_d(s, z) = \frac{4}{3}\pi\rho_s s_0^3 n_d(s_0, z) = \rho_d(s_0, z). \quad (35)$$

In the case with $p = -3$, equation (35) shows that initial density of dust with different radius is the same. In this case, $\rho_d(s, z)$ is given by

$$\rho_d(s, z) = \frac{1}{N_d}\rho_d(z) = \frac{1}{N_d}\frac{\Sigma_d}{\sqrt{\pi}H_{d,s}}\exp\left[-\left(\frac{z}{H_{d,s}}\right)^2\right]. \quad (36)$$

In the case without dust growth, $\rho_d(s, z)$ with different s evolves independently, with different $H_{d,s}$. From equations (32), (33) and (36), we can derive analytical solutions of $\rho_d(z)$. We assume $N_d = 1000$.

Figure 3 shows dust density and Richardson number for the case with $f_d = 50$. In Figure 3, it is seen that dust density at the midplane attains the critical density ρ_c , and that Richardson number remains larger than the critical value. This demonstrates that dust fraction 50 times larger than MMSN model induces GI before KHI in the case without dust growth. Note that this dust fraction is about 10 times smaller than that in Figure 2. We checked the dependence on N_d and found that this is the case with for $N_d \gtrsim 10$. Thus, it can be suggested that KHI tends to be inhibited before GI if dust grains have size distribution even with the same f_d . The reason is that the vertical gradient of dust density becomes smaller as a result of the continuous size distribution.

Figure 4 shows dust density in the midplane at the onset of KHI for the both cases without and with size distribution. The symbol $\rho_{d,KH}$ is the dust density in the midplane at the onset of KHI. It is seen that dust density in the midplane at the onset of KHI increases with increasing the dust abundance in both cases with and without size distribution. Especially, it is seen that the condition $\rho_{d,KH} = \rho_c$ is attained by smaller dust abundance f_d in the case with size distribution $f_d > 50$ than without size distribution $f_d \gtrsim 700$.

Above results are based on $Ri_c = 0.25$ (Chandrasekhar 1961). However, Johansen et al. (2006) showed that $Ri_c = 0.8$. We also investigated the case with $Ri_c = 0.8$. In the case

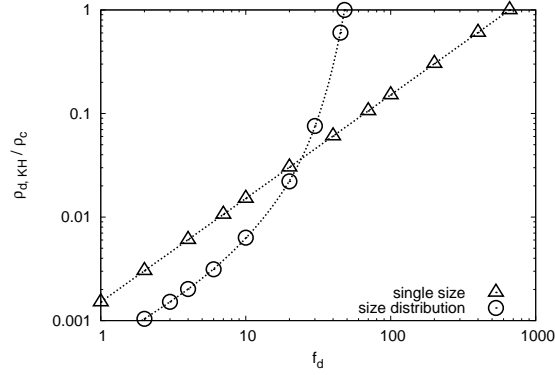


Fig. 4. The dust density in the midplane and in $r = 1$ AU at the onset of KHI for the case without size distribution of dust grains (triangles) and for the case with size distribution of dust grains (circles). The abscissa shows dust abundance f_d , and the ordinate shows the dust density $\rho_{d,KH}$ in unit of ρ_c . The approximated curves are also drawn (dotted lines).

without size distribution, the required abundance of dust for GI is about 1.2×10^3 . On the other hand, in the case with size distribution, the required abundance is smaller than 100. This abundance is much smaller than that for the case without size distribution, and this result is qualitatively same as that for the case with $Ri_c = 0.25$. Thus, below, we concentrate on the case with $Ri_c = 0.25$.

In the case without dust growth, results are summarized as follows:

1. In the case when the abundance of dust grains is given as MMSN model, KHI is expected to occur when dust density at the midplane is still much smaller than the critical density for GI.
2. GI tends to occur if the abundance of dust grains is larger.
3. If dust grains have the initial size distribution, the required abundance of dust for GI has the possibility to be smaller than that in the case without size distribution.

Above results are based on the assumption that dust grains don't grow and that initial size distribution is assumed. However, in the actual protoplanetary disks, dust grains are expected to collide mutually and to grow. If dust grains grow, the size distribution and the largest radius of dust grains will change with time. In order to understand the actual condition of dust abundance for GI, size distribution which is consistent with dust growth during sedimentation is desirable. Next, we consider the case with dust growth.

4. The case with dust growth

4.1. The initial condition and the numerical method

We investigate sedimentation and growth of dust grains at $r = 1$ AU in the case with $f_g = 1$. We solve equation (16) numerically. We assume that the internal density of dust

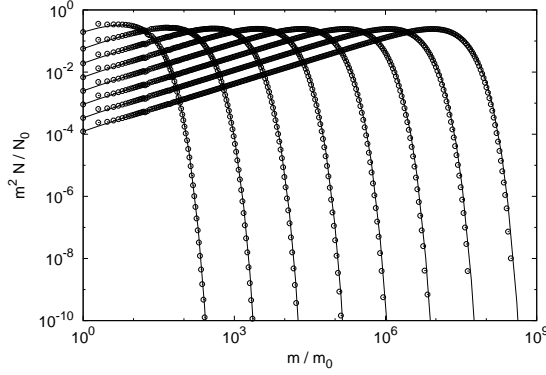


Fig. 5. Results of the test of our numerical method for growth of dust grains. Numerical results (circles) are compared with analytic solutions by Trubnikov (1971) (solid lines).

grains ρ_s is 3.0 g cm^{-3} . As initial condition, we assume that all dust grains have the initial size $s_0 = 1.0 \times 10^{-4} \text{ cm}$ and initial density given by equation (24).

In numerical calculations, TVD scheme (Roe 1986) is applied to calculate sedimentation of dust grains and the method of WS89 (Wetherill & Stewart 1989) is applied for dust growth. The mass coordinates m_i are logarithmically divided into 400 mass bins. Our numerical method is tested using the analytical solution (Trubnikov 1971). Figure 5 shows results with our numerical method for growth of dust grains. In Figure 5, it is seen that our numerical method has satisfactory accuracy to calculate growth of dust grains. The z coordinates z_j are logarithmically divided into 106 spaced grids. The thickness of the nearest grid to the midplane is $1.4 \times 10^{-8} H_g$. Using this spatial resolution, scale height at GI is sufficiently resolved.

4.2. Possibilities of KHI in the early stage

Figure 6 shows the distribution of dust density and Richardson number at $t = 25$ year. In Figure 6, although the distribution of dust density changes little from the initial state in this short period, it is seen that Richardson number becomes small enough in small z especially $z/H_g \lesssim 10^{-4} \ll 1$. This rapid decline of Ri did not come out in the case without growth of dust grains in §3. We suppose that growth of dust grains is the origin of this rapid decline in Richardson number at $z/H_g \ll 1$ and at $t/t_{\text{sed}} \ll 1$.

Equations (12) and (15) show that Richardson number is a function of the gradient of dust density $\partial \rho_d(z)/\partial z$, so we now think about $\partial \rho_d(z)/\partial z$. First, we think about the case without growth of dust grains to evince the effect of dust growth. We think about the case when all dust grains have a single size as initial condition because we assume that all dust grains have an initial radius s_0 as initial condition for the calculation in the case with dust growth. In the case without growth and size distribution of dust grains, the typical radius of dust grains $\bar{s}(z)$, which is defined as

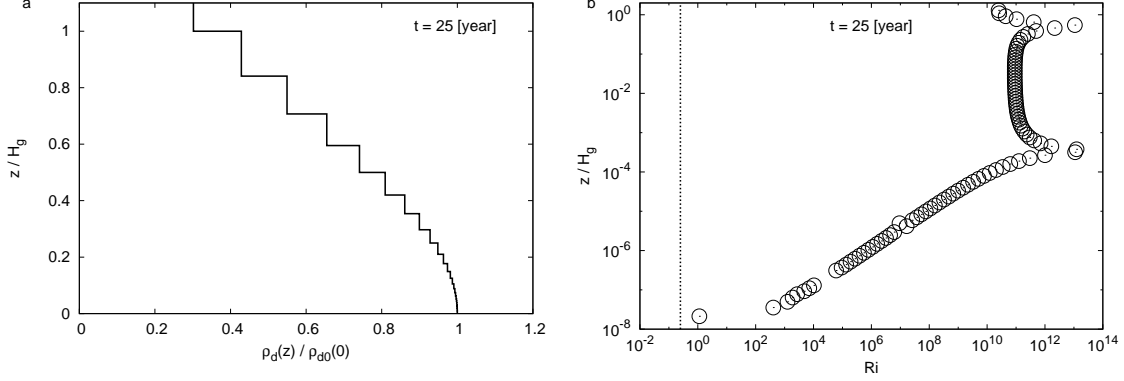


Fig. 6. (a) The distribution of dust density at $r = 1$ AU and at $t = 25$ year. The line, the abscissa and the ordinate show the same as ones of Figure 1 (a). (b) The distribution of Richardson number at $t = 25$ year. The abscissa shows Richardson number. The ordinate shows z coordinates in unit of H_g . The critical value Ri_c is also drawn (dotted line).

$$\bar{s}(z) \equiv \frac{\int_0^\infty s mn(m, z) dm}{\int_0^\infty mn(m, z) dm}, \quad (37)$$

is equal to s_0 and is independent on z . Garaud & Lin (2004) shows that time dependence of dust density proceeds in the self-similar manner in the case without growth of dust grains. In this case, the gradient of dust density is given by

$$\frac{\partial \rho_d(z)}{\partial z} = -\frac{2\Sigma_d z}{\sqrt{\pi} H_d^3} \propto z \rightarrow 0 \quad (z \rightarrow 0). \quad (38)$$

In order to compare with the case with growth of dust grains, we think about the sedimentation velocity for the gravity center of the dust system at z , $\bar{v}_z(z)$, which is derived from equations (11), (23) and (37). At $z/H_g \ll 1$ and at $t/t_{\text{sed}} \ll 1$, $\bar{v}_z(z)$ is given by

$$\bar{v}_z(z) \equiv -\frac{\rho_s}{\rho_g(z)} \frac{\bar{s}(z)}{c_s} \Omega_K^2 z. \quad (39)$$

In the case without growth of dust grains, $\bar{v}_z(z) \propto z$ at $z/H_g \ll 1$ because $\bar{s}(z) = s_0$.

Second, we think about the case with growth of dust grains. In this case, the typical radius of dust grains $\bar{s}(z)$ is the linear function of z at $z/H_g \ll 1$ and at $t/t_{\text{sed}} \ll 1$ owing to collisions due to sedimentation (see Appendix for the reason). From equation (39), $\bar{v}_z(z)$ has a second-order term of z because the typical radius of dust grains is the linear function of z . From comparing the functional form of $\bar{v}_z(z)$ with that in the case without dust growth, at $z/H_g \ll 1$ and at $t/t_{\text{sed}} \ll 1$, it is suggested that the gradient of dust density is given by

$$\frac{\partial \rho_d(z)}{\partial z} = \delta_1 z + \delta_2 \rightarrow \delta_2 \quad (z \rightarrow 0), \quad (40)$$

where $\delta_1 (< 0)$ and $\delta_2 (> 0)$ are appropriate values.

Figure 7 shows the distribution of the gradient of the dust density at $z/H_g \ll 1$ and at $t = 25$ year for cases with and without dust growth. From Figure 7, it is confirmed that the

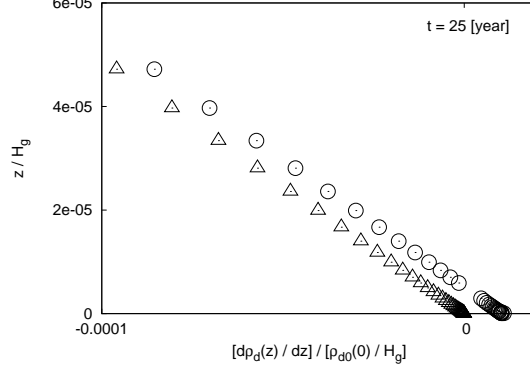


Fig. 7. The distribution of the gradient of dust density in $r = 1$ AU and $z/H_g \ll 1$ at $t = 25$ year. The abscissa shows the gradient of dust density $\partial \rho_d(z)/\partial z$ in unit of $\rho_{d0}(0)/H_g$. The ordinate shows z coordinates in unit of H_g . Circles show the case with dust growth and triangles show the one without dust growth.

distribution of the gradient of dust density is approximated by equation (40) with $\delta_2 > 0$ in the case with dust growth. From Figure 7, we can approximate $\partial \rho_d(z)/\partial z \simeq [-2.0(z/H_g) + 1.0 \times 10^{-5}][\rho_{d0}(0)/H_g]$. This indicates that the distribution of dust density has a local maximum value at $z/H_g \sim 5 \times 10^{-6}$ in the case with growth of dust grains. This can be confirmed by seeing Figure 8 that shows the distribution of dust density in $z/H_g \ll 1$ and at $t = 25$ year in the case with dust growth. By approximating $\rho_g(z)$ as $\rho_g(0)$ and $\rho_d(z)$ as $\rho_{d0}(0)$, the Richardson number for $z/H_g \ll 1$ is given by

$$\text{Ri} = \left(\frac{16}{13}\right)^2 \left(\frac{r}{H_g}\right)^2 \left(\frac{\Sigma_g}{\Sigma_d}\right)^{-2} \left(\frac{\Sigma_g}{\Sigma_d} + 1\right)^3 \times \frac{z}{H_g} \left[\frac{2\Sigma_g}{\Sigma_d} \frac{z}{H_g} - \frac{\partial \rho_d(z)}{\partial z} \frac{H_g}{\rho_{d0}(0)} \right] \left[\frac{2z}{H_g} + \frac{\partial \rho_d(z)}{\partial z} \frac{H_g}{\rho_{d0}(0)} \right]^{-2}. \quad (41)$$

Figure 9 shows the distribution of Richardson number at $z/H_g \ll 1$ and at $t = 25$ year in the case with growth of dust grains. In Figure 9, it is seen that numerical solutions of Richardson number is sufficiently close to the approximate equation (41). In Figure 9, it is seen that Richardson number drawn by the solid line is smaller than the critical value Ri_c around the midplane at $t = 25$ year.

However, it is doubtful whether KHI occurs. In Figure 8, it is seen that the distribution of dust density has a local maximum value at $z \neq 0$. Under the local maximum point, the Rayleigh-Taylor instability (RTI) is suspected to occur because the distribution of the gradient of dust density becomes positive (Chandrasekhar 1961). If RTI occurs, the distribution of dust density in this region is expected to be adjusted as to be constant (Sekiya & Ishitsu 2001). If it is assumed that the growth rate of RTI is larger than that of KHI, and that the distribution of dust density becomes constant around the midplane, the gradient of dust density becomes zero near the midplane. In this case with assuming that gas density is given by equation (5),

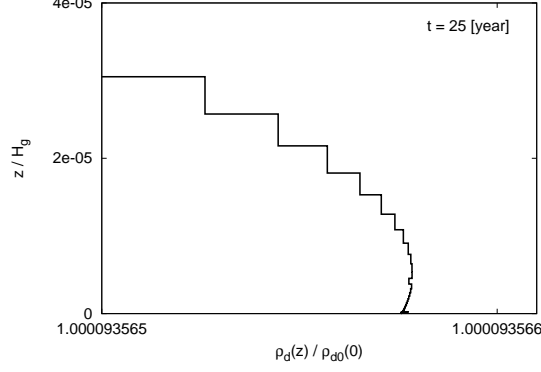


Fig. 8. The distribution of dust density in $r = 1$ AU and $z/H_g \ll 1$ at $t = 25$ year in the case with growth of dust grains. The line, the abscissa and the ordinate show the same as ones of Figure 1 (a).

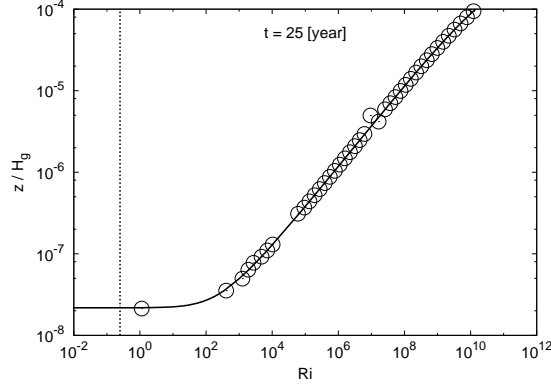


Fig. 9. The distribution of Richardson number in $r = 1$ AU and $z/H_g \ll 1$ at $t = 25$ year in the case with growth of dust grains. Circles, the dotted line, the abscissa and the ordinate show the same as ones of Figure 6 (b). The solid line is given by equation (41).

Richardson number near the midplane is given by

$$\text{Ri} = \frac{128}{169} \left(\frac{r}{H_g} \right)^2 \frac{(\Sigma_g + \Sigma_d)^3}{\Sigma_g \Sigma_d^2} \sim 2 \times 10^7 \gg 0.25 = \text{Ri}_c. \quad (42)$$

This indicates that KHI does not occur. Thus, below, the possibility of KHI near the midplane in the early phase as indicated in Figure 6 (b) is not considered further.

4.3. The dust density at the onset of KHI for the case with dust growth

Figure 10 shows dust density distribution at the onset of KHI in the case with dust growth with $f_d = 1$. In Figure 10 (a), distribution of dust density has a local maximum value at $z = z_{\text{RT}} \sim 10^{-3} H_g$, and there is the region where the gradient of dust density becomes positive. As discussed in §4.2, in this case, the distribution of dust density is expected to be adjusted to be constant by RTI in the region $z \lesssim z_{\text{RT}}$. Assuming this RTI, we modify the distribution of dust density as Figure 10 (b) with mass conservation. Note that this treatment for RTI is crude

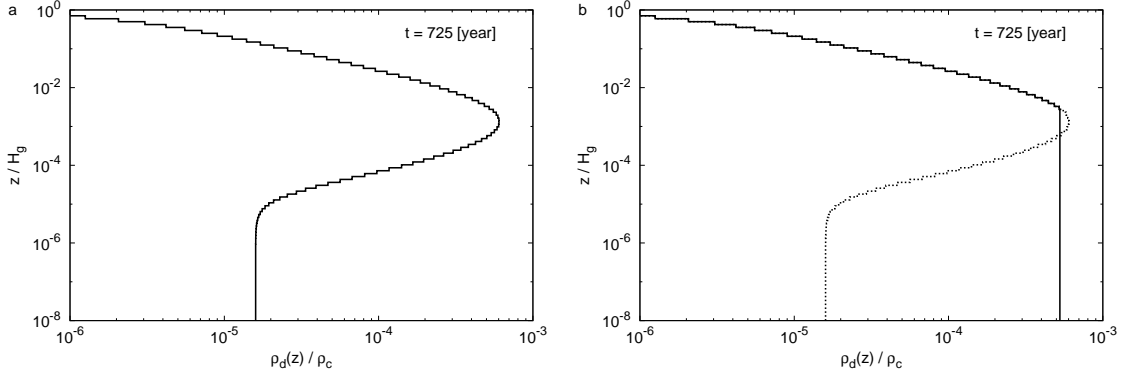


Fig. 10. Dust density in $r = 1$ AU at the onset of KHI for the case with dust growth and $f_d = 1$. (a) The dust density obtained by numerical calculations. (b) The dust density adjusted as to be constant (solid line) and the dust density not adjusted (dotted line). The dust density not adjusted is equal to the one obtained by numerical calculations. For both of Figure (a) and (b), the abscissas show the dust density $\rho_d(z)$ in unit of ρ_c , and the ordinates show z coordinates in unit of H_g .

and more accurate treatment should be addressed in the future. Hereafter, same modification is always applied for the density near the midplane.

Figure 11 shows the modified dust density profile at the onset of KHI. Figure 11 corresponds to Figure 4 with dust growth. Since the case with large f_d is numerically expensive, results only for the case with $f_d \leq 4$ are plotted. In Figure 11, it is seen that dust density at KHI, $\rho_{d,KH}$, increases with increasing dust abundance for the case with $f_d < 2$. On the other hand, in the case with $f_d > 2$, it is seen that dust density at KHI decreases with increasing dust abundance. This tendency is qualitatively different from Figure 4. In Figure 11, our results show that dust density in the midplane at the onset of KHI for the case with $f_d = 4$ is about the same as that for the case with $f_d = 1$. As the physical origin of the decline of $\rho_{d,KH}$ for $f_d > 2$, we consider the difference of property of gas drag. After dust grains grow, the law of gas drag changes from Epstein's law to Stokes' law. Figure 12 shows the mass function at the onset of KHI at the maximum density for the case with $f_d = 1$ and $f_d = 4$, respectively. For the case with $f_d = 1$, the mass function has the peak at $m/m_0 \sim 10^{12}$ and the typical size of dust grains is 0.9 cm. On the other hand, for the case with $f_d = 4$, the mass function has the peak at $m/m_0 \sim 10^{14}$ and the typical radius of dust grains is 4 cm. In the case with $s \geq 3l_g/2 = 2.2$ cm, the stopping time is given by Stokes' law. By comparison of these results, it is suggested that the decrease of dust density at KHI for $f_d > 2$ in Figure 11 originates from the change of the law of gas drag due to dust growth.

To confirm this possibility, for reference, we recalculate the evolution using Epstein's law for all size. Solid line in Figure 13 shows the dust density at the onset of KHI for this case. It is clearly seen that the dust density at the onset of KHI increases with increasing f_d . By comparing two lines in Figure 13, it is clear that the physical origin for the decline of $\rho_{d,KH}$ for

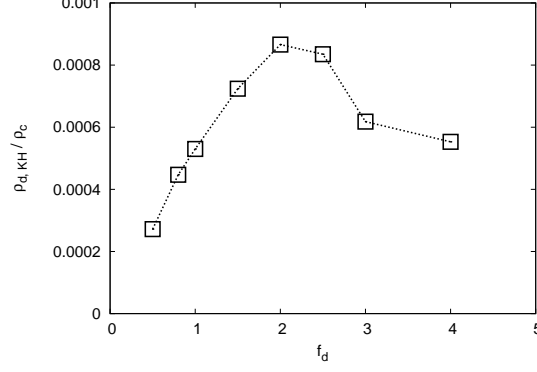


Fig. 11. The modified dust density in $r = 1$ AU at the onset of KHI for the case with dust growth. The abscissa and the ordinate show the same as ones of Figure 4.

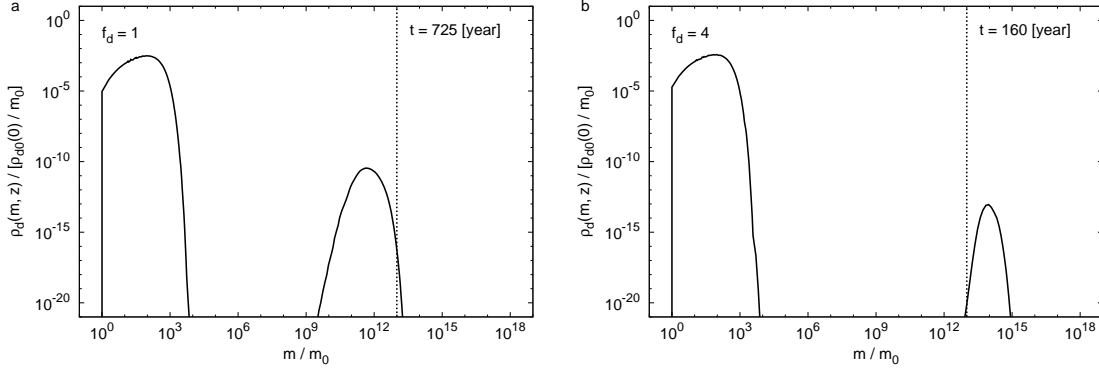


Fig. 12. (a) The mass function in the case with $f_d = 1$ at $z = 1.5 \times 10^{-3} H_g$ and $r = 1$ AU where the distributions of dust density takes a local maximum value at the onset of KHI. (b) The mass function in the case with $f_d = 4$ at $z = 3.8 \times 10^{-4} H_g$ and $r = 1$ AU where the distributions of dust density takes a local maximum value at the onset of KHI. In both of diagrams (a) and (b), The abscissa shows the dust mass m in unit of m_0 . The ordinate shows the mass function $mn(m, z)$ in unit of $\rho_{d0}(0)/m_0$. Dotted lines show the border line, where the stopping time changes from Epstein's law to Stokes' law.

$f_d > 2$ is the change of gas drag from Epstein's law to Stokes' law. Therefore, it is significant for us to take into account the dust size dependence of the stopping time as well as dust growth when we investigate the shear-driven turbulence in the protoplanetary disk.

5. Discussion

5.1. Dependence on the heliocentric distance

We estimate the dependence of the required abundance of dust for GI on the heliocentric distance r . First, we consider the case without dust growth. For simplicity, we consider the case when all dust grains have a single size. The scale height of dust density profile at the onset of KHI can be obtained from equation (30), and we define the scale height as H_{KHI} . With

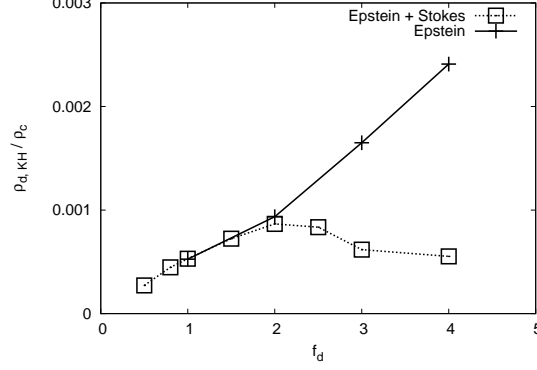


Fig. 13. The modified dust density in $r = 1$ AU at the onset of KHI for the case with dust growth in cases of using both Epstein's law and Stokes' law (dotted line and squares), and using only Epstein's law for all size (solid line and crosses). The abscissa and the ordinate show the same as ones of Figure 4.

substituting Ri_c and H_{KHI} for $\text{Ri}(z = z_c)$ and H_d in equation (30), respectively, H_{KHI} is given by

$$H_{\text{KHI}} = \left(\frac{8\text{Ri}_c}{27} \right)^{\frac{1}{2}} \eta r = 1.0 \times 10^{-2} H_g \left(\frac{r}{1[\text{AU}]} \right)^{\frac{1}{4}}. \quad (43)$$

Equation (43) shows that H_{KHI} is independent on f_d . The dependence of H_c (defined in equation (27)) on r is given by $H_c = 1.6 \times 10^{-5} f_d \xi_{\text{ice}} H_g (r/1 [\text{AU}])^{1/4}$, and we have

$$\frac{H_{\text{KHI}}}{H_c} = 6.6 \times 10^2 \left(\frac{f_d}{1} \right)^{-1} \left(\frac{\xi_{\text{ice}}}{1} \right)^{-1}. \quad (44)$$

The parameter of condensed water ice ξ_{ice} is given by 1 (at $r < 2.7$ AU) or 4.2 (at $r > 2.7$ AU) (Hayashi 1981; Hayashi et al. 1985). Equation (44) shows the possibility that the required abundance of dust for GI is smaller outside the snow line than inside. Next, we consider the case with dust growth. At the onset of KHI, most of the dust grains with the typical size calculated in §4.3 (defined in equation (37)) have settled near the midplane. Thus, the typical size of dust at the onset of KHI can be obtained as the size of dust grains which have settled from high altitudes to the midplane. As Safronov (1969), we have $dm = 4\pi s^2 \rho_s ds \sim -p_s \pi (2s)^2 \rho_d(z) dz$. Assuming that $s = s_0$ at $z = +\infty$ and that $s = s_f \gg s_0$ at $z = 0$, we derive s_f as

$$s_f \sim \frac{p_s \Sigma_d}{2\rho_s} \sim \left(\frac{f_d}{1} \right) \left(\frac{\xi_{\text{ice}}}{1} \right) \left(\frac{r}{1[\text{AU}]} \right)^{-\frac{3}{2}} [\text{cm}]. \quad (45)$$

The typical sizes of dust at the onset of KHI calculated in §4.3 were 0.9 cm and 4 cm in the case with $f_d = 1$ and $f_d = 4$, respectively, and consistent with equation (45). Equation (45) shows that the typical size of dust at the onset of KHI is smaller for larger r . On the other hand, the mean free path of gas molecules scales as $l_g \propto \rho_g^{-1} \propto H_g \Sigma_g^{-1} \propto r^{11/4}$, and l_g is larger for larger r . Thus, the gas drag force tends to be given by Epstein's law in the outer region of protoplanetary disk even for a large f_d . The Solid line in Figure 13 shows that the dust density

at the onset of KHI is larger for larger f_d in the Epstein regime. Therefore, the outer region of the protoplanetary disk might be more suitable for GI than the inner region.

Above discussion is different from that in Takeuchi et al. (2012) that showed that the inner part of the protoplanetary disk is more suitable for GI. Takeuchi et al. (2012) is based on the different condition from ours. Takeuchi et al. (2012) used the scale height of the dust layer which is determined by the balance between sedimentation and diffusion of dust grains, while we used the scale height of dust density profile at the onset of KHI.

5.2. *The linear analysis of the shear instability*

In this paper, we used Richardson number as an indicator of KHI in order to discuss the possibility of the shear-driven turbulence. However, although KHI occurs, there is a possibility that some dust grains continue to settle toward the midplane if the shear-induced turbulence is weak. An analysis with only Richardson number is insufficient in order to understand the effect of the shear-induced instability in the protoplanetary disk. Sekiya & Ishitsu (2001) and Michikoshi & Inutsuka (2006) calculated the growth rate of the shear-induced instability by solving the linear perturbation equations. In these studies, the growth rate of the shear-induced instability depends on the assumed distribution of dust density which is not consistent with the formation process of dust layer. Thus, it would be better to calculate the growth rate of KHI as well as RTI with the consistent density distribution that is given in this paper. This will be addressed in the forthcoming paper.

5.3. *Possibilities of the streaming instability and the fractal growth of dust*

Youdin & Goodman (2005) and Johansen & Youdin (2007) showed that the dynamics in the midplane is dominated by the streaming instability. Bai & Stone (2010) showed that dust grains with $\tau_s \equiv \Omega_K t_{\text{stop}} > 0.01$ trigger the streaming instability before KHI. In our model, at $r = 1$ AU, $\tau_s > 0.01$ corresponds to $s > 2$ cm. For our calculations, for the case with dust growth and $f_d > 2$, the typical size of dust grains at the maximum density is larger than 2 cm. Therefore, in the dust layer governed by Stokes' law, the streaming instability would occur before KHI and GI.

In this paper, we assumed compact and spherical dust grains. However, since dust grains grow due to dust-dust collisions, large dust grains are aggregates of small dust grains. Both laboratory and numerical experiments show that aggregates are not at all compact and spherical, but have a fluffy structure (Wurm & Blum 1998; Kempf et al. 1999; Okuzumi et al. 2009). With the same mass, the radius of the fractal aggregate is larger than the radius of the compact and spherical dust grain, and varies with the porosity of the aggregate. Therefore, it is essential to investigate the evolution of porosity during the growth of dust aggregate.

6. Conclusion

In this paper, we considered the sedimentation and the growth of dust grains, and we discussed the possibility of the shear-driven turbulence during dust sedimentation with and without dust growth. We assumed that the gas component is in hydrostatic equilibrium and that gas are not affected by motion of dust grains. Dust grains are assumed to be compact and spherical, and radial motion of dust grains are neglected. We used a single-fluid approximation for the azimuthal motion. For dust-dust collisions, it is assumed that dust grains collide and coalesce by sedimentation or the thermal Brownian motion.

Our study shows the following results: (1) The shear-driven turbulence is expected to occur before the onset of the gravitational instability in MMSN model at $r = 1$ AU. (2) In the case without dust growth, at the onset of KHI, dust density in the midplane is large for larger dust abundance. This tendency holds for the same initial size distribution of dust grains. (3) In the case with dust growth, dust density at the onset of KHI decreases with increasing dust abundance with $f_d > 2$. This result is qualitatively different from the one in the case without dust growth. The reason is that gas drag changes from Epstein's law to Stokes' law for larger dust grains which grow up in advance. Thus, we stress that, for the study of shear-driven turbulence, the change of the law of gas drag from Epstein's law to Stokes' law as well as dust growth is required to be taken into account.

For the formation of planetesimals, it has been suggested that in order to occur GI before inward drift of dust, dust grains have to settle toward the midplane, and it is suggested to possible with large dust abundance. However, in this paper, it is suggested that the shear-driven turbulence is certain to happen even if dust abundance in the protoplanetary disk is larger than MMSN model. In future work, we should develop a more realistic model with calculating the effect of KHI and RTI directly.

We thank Fumio Takahara for fruitful discussion and continuous encouragement. We also acknowledge discussion with Sugawara in the early stage of this work.

Appendix. The typical radius of dust grains in the case with dust growth

We explain the reason that the typical radius of dust grains $\bar{s}(z)$ is the linear function of z at $z/H_g \ll 1$ and at $t/t_{\text{sed}} \ll 1$ owing to collisions due to sedimentation in the case with growth of dust grains. We now estimate the mean collision time in the same method used in Nakagawa et al. (1981). The mean collision time is given by

$$t_{\text{coll}} = \frac{1}{n_d \sigma \Delta v}, \quad (\text{A1})$$

where n_d is the number density of dust grains, σ is the collisional cross section and Δv is the relative velocity of the dust-dust collision. We assume that radii of dust grains are given by the typical radius and that masses of dust grains are given by the typical mass of dust grains.

The typical mass is given by

$$\bar{m}(z) = \frac{4}{3}\pi\rho_s[\bar{s}(z)]^3, \quad (\text{A2})$$

and we regard that $\sigma = \pi\bar{s}^2$. We treat n_d as ρ_d/\bar{m} or $(\Sigma_d/\Sigma_g)[\rho_g/\bar{m}]$ at $z/H_g \ll 1$ and at $t/t_{\text{sed}} \ll 1$. For the collision due to sedimentation, we simply put $|s - s'| = \bar{s}$ and $\Delta v = \Delta v_s$. The mean collision time for sedimentation is defined as $t_{\text{coll},s}$. At $z/H_g \ll 1$ and at $t/t_{\text{sed}} \ll 1$, $t_{\text{coll},s}$ is obtained by

$$t_{\text{coll},s} = \frac{2\sqrt{2}\Sigma_g}{3\Sigma_d\Omega_K} \left(\frac{z}{H_g}\right)^{-1} = 36 \left(\frac{z}{H_g}\right)^{-1} [\text{year}]. \quad (\text{A3})$$

In equation (A3), it is seen that $t_{\text{coll},s}$ is independent of \bar{s} and $t_{\text{coll},s} \propto z^{-1}$ at $z/H_g \ll 1$ and at $t/t_{\text{sed}} \ll 1$. For the collision due to the thermal motion, we simply put $m = m' = \bar{m}$ and $\Delta v = \Delta v_B$. The mean collision time for the thermal motion, $t_{\text{coll},B}$, is obtained by

$$t_{\text{coll},B} = \frac{4}{3} \sqrt{\frac{2}{3}} \frac{\pi H_g \rho_s^{\frac{3}{2}} s_0^{\frac{5}{2}}}{\Sigma_d \sqrt{k_B T}} \left(\frac{\bar{s}}{s_0}\right)^{\frac{5}{2}} \exp \left[\left(\frac{z}{H_g} \right)^2 \right] = 28 \left(\frac{\bar{s}}{s_0}\right)^{\frac{5}{2}} [\text{year}], \quad (\text{A4})$$

at $z/H_g \ll 1$ and at $t/t_{\text{sed}} \ll 1$. In equation (A4), it is seen that $t_{\text{coll},B}$ is independent of z and $t_{\text{coll},B} \propto \bar{s}^{5/2}$ at $z/H_g \ll 1$ and at $t/t_{\text{sed}} \ll 1$.

From equations (A3) and (A4), it is found that $t_{\text{coll},B} < t_{\text{coll},s}$ while radii of dust grains are relatively small. Therefore, it is suggested that collisions due to the thermal motion is dominant as long as radii of dust grains are relatively small. After dust grains have grown, it is expected that $t_{\text{coll},B} > t_{\text{coll},s}$, and that collisions due to sedimentation are dominant. The growing speed of dust grains in sedimentation is expected to be proportional to z because $t_{\text{coll},s} \propto z^{-1}$. Thus, it is supposed that the typical mass of dust grains at z , $\bar{m}(z)$, is given by $\bar{m}(z) = [a_1(z/H_g) + a_2]m_0$, where a_1 and a_2 are appropriate values. Then, the typical radius of dust grains at z is given by $\bar{s}(z) = [a_1(z/H_g) + a_2]^{1/3}s_0$. If $a_1z/a_2H_g \ll 1$, it is supposed that $\bar{s}(z)$ is approximated by $[a_3(z/H_g) + a_4]s_0$ with Taylor expansion. Symbols a_3 and a_4 are appropriate values.

Figure 14 shows the distribution of the typical mass and radius of dust grains at $z/H_g \ll 1$ and at $t = 25$ year. From Figure 14, it is confirmed that $\bar{s}(z) = [a_3(z/H_g) + a_4]s_0$ at $z/H_g \ll 1$ and at $t/t_{\text{sed}} \ll 1$.

Above discussions assume that collisions due to sedimentation become more dominant than those due to the thermal motion immediately. However, it is not confirmed that collisions due to sedimentation is dominant to growth of dust grains before $t = 25$ year. We now should confirm that this assumption is appropriate for the case that we investigate.

At $z/H_g \ll 1$ and $t \approx 0$, it is expected that collisions due to the thermal motion is dominant and $t_{\text{coll},B}$ is independent of z . In this case, it is supposed that the typical radius of dust grains is independent of z , i.e., a_3 in the formula for $\bar{s}(z)$ is temporally constant. However, in a certain time, it is expected that the dominant effect in the growth of dust grains changes from collisions due to the thermal motion to those due to sedimentation because of dust growth.

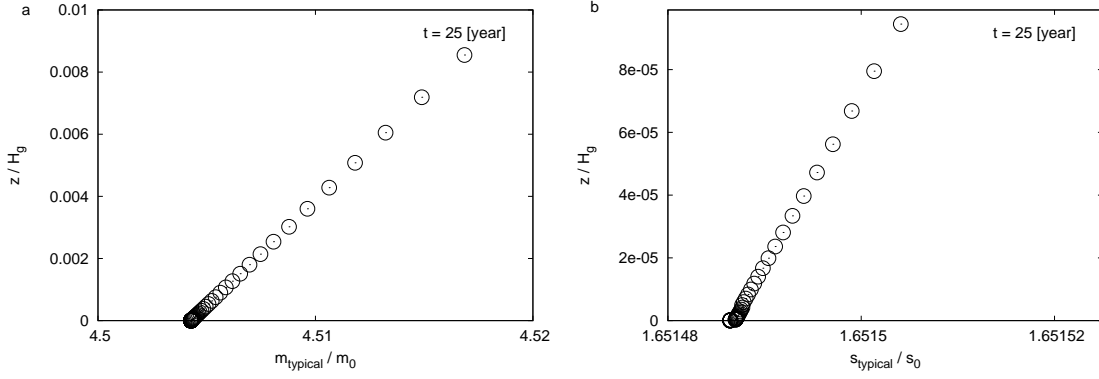


Fig. 14. (a) The distribution of the typical mass of dust grains in $r = 1$ AU at $t = 25$ year. The abscissa, where m_{typical} means \bar{m} , shows the typical mass \bar{m} in unit of m_0 . The ordinate shows z coordinates in unit of H_g . (b) The distribution of the typical radius of dust grains at $t = 25$ year. The abscissa, where s_{typical} means \bar{s} , shows the typical radius \bar{s} in unit of s_0 . The ordinate shows z coordinates in unit of H_g .

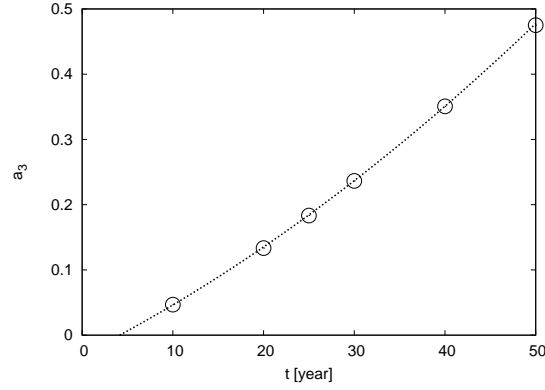


Fig. 15. The time development of a_3 (Circles) in $r = 1$ AU and $z / H_g \ll 1$ at $t / t_{\text{sed}} \ll 1$. The abscissa shows time and the ordinate shows a_3 that is derived from fitting $\bar{s}(z)$ into $[a_3(z / H_g) + a_4]s_0$. The approximated curve is also drawn (dotted line).

Therefore, the time for this change can be determined by investigating the time development of a_3 for $\bar{s}(z)$.

Figure 15 shows the time development of a_3 . From Figure 15, a_3 is approximated by $a_3 = 6.3 \times 10^{-5}(t/1 \text{ [year]})^2 + 7.0 \times 10^{-3}(t/1 \text{ [year]}) - 3.0 \times 10^{-2}$. This shows that $a_3 > 0$ at $t \gtrsim 4$ year, so it is considered that collisions due to sedimentation dominate in growth of dust grains at $t \gtrsim 4$ year. Therefore, we show that the assumption that collisions due to sedimentation become more dominant to growth of dust grains than those due to the thermal motion immediately is proper to the case that we investigate.

References

- Adachi, I., Hayashi, C., & Nakazawa, K. 1976, *Prog. Theor. Phys.*, 56, 1756
- Bai X., & Stone J. M. 2010, *ApJ*, 722, 1437
- Chandrasekhar, S. 1961, *Hydrodynamic & Hydromagnetic Stability* (New York: Dover)
- Cuzzi, J., Dobrovolskis, A., & Champney, J. 1993, *Icarus*, 106, 102
- Dobrovolskis, A. R., Dacles-Mariani, J. S., & Cuzzi, J. N. 1999, *J. Geophys. Res.*, 104, 30805
- Garaud, P., & Lin, D. N. C. 2004, *ApJ*, 608, 1050
- Goldreich, P., & Ward, W. 1973, *ApJ*, 183, 1051
- Gómez, G. C., & Ostriker, E. C. 2005, *ApJ*, 630, 1093
- Hayashi, C. 1981, *Prog. Theor. Phys. Suppl.*, 70, 35
- Hayashi, C., Nakazawa, K., & Nakagawa, Y. 1985, in *Protostars & Planets II*, ed. D. C. Black & M. S. Mathews (Tucson: Univ. Arizona Press), 1100
- Johansen, A., Henning, Th., & Klahr, H. 2006, *ApJ*, 643, 1219
- Johansen, A., & Youdin, A. 2007, *ApJ*, 662, 627
- Kempf, S., Pfalzner, S., & Henning, T. K. 1999, *Icarus*, 141, 388
- Michikoshi, S., & Inutsuka, S. 2006, *ApJ*, 641, 1131
- Nakagawa, Y., Nakazawa, K., & Hayashi C. 1981, *Icarus*, 45, 517
- Nakagawa, Y., Sekiya, M., & Hayashi C. 1986, *Icarus*, 67, 375
- Okuzumi, S. 2009, *ApJ*, 698, 1122
- Okuzumi, S., Tanaka, H., & Sakagami, M.-a. 2009, *ApJ*, 707, 1247
- Roe, P. L. 1986, *Ann. Rev. Fluid Mech.*, 18, 337
- Safronov, V. S. 1969, *Evolution of the Protoplanetary Cloud & the Formation of the Earth & Planets* (Moscow: Nauka Press)
- Sekiya, M. 1983, *Prog. Theor. Phys.*, 69, 1116
- Sekiya, M. 1998, *Icarus*, 133, 298
- Sekiya, M., & Ishitsu, N. 2001, *Earth Planets Space*, 53, 761
- Takeuchi, T., Muto, T., Okuzumi, S., Ishitsu, N., & Ida, S. 2012, *ApJ*, 744, 101
- Trubnikov, B. A. 1971, *Sov. Phys. Dokl.*, 16, 124
- Weidenschilling, S. J. 1980, *Icarus*, 44, 172
- Wetherill, G. W., & Stewart, G. R. 1989, *Icarus*, 77, 330
- Wurm, G., & Blum, J. 1998, *Icarus*, 132, 125
- Youdin, A. N., & Goodman, J. 2005, *ApJ*, 620, 459
- Youdin, A. N., & Shu, F. H. 2002, *ApJ*, 580, 494
- Zsom, A., Ormel, C. W., Güttler, C., Blum, J., & Dullemond, C. P. 2010, *A&A*, 513, A57